Supplementary Information (SI) for Materials Chemistry Frontiers.
This journal is © the Partner Organisations 2026

Supplementary Information

Design and Nonlinear Optical Properties of Benzotrithiophene-Based Covalent Organic Frameworks

Jianhong Jia*, Ran Yao, Jiawei Du, Mingyan Li, Jiahui Chu, Huilin Zhao, Ziqi Li, Debo Ding and Yunfang Yang

College of Chemical Engineering, Zhejiang University of Technology, Hangzhou 310014, China

* Corresponding author (email: zgdjjh@163.com)

Table of Contents

1. Materials and methods

Reagents: All chemical reagents and solvents employed in this work were either commercially available and used without further purification or synthesized in accordance with the previously reported protocols detailed herein.

Solution nuclear magnetic resonance (NMR): Liquid state ^{1}H and ^{13}C nuclear magnetic resonance spectroscopy were measured on a Varian Mercury Plus 400 NMR Spectrometer.

High resolution mass spectrometry (HRMS): The electrospray ionization mass spectrometry (ESI-MS) spectra were recorded using a Sciex X500R QTOF MS spectrometer.

Fourier transform infrared (FT-IR): IR spectrum was measured on an IR spectrometer (Nicolet 6700) between the ranges of 4000 to 400 cm^{-1}.

Solid-state nuclear magnetic resonance (ssNMR): Solid-state NMR spectra were performed on a Bruker 400M spectrometer with cross-polarization magic-angle-spinning (CP/MAS) at a resonance frequency of 150.9 MHz. ^{13}C CP/MAS NMR spectra were recorded using a 4 mm MAS probe and a spinning rate of 10 kHz. A contact time of 4 s and a recycle delay of 6.5 μs were used for the ^{13}C CP/MAS NMR measurement. The chemical shifts of ^{13}C were externally referenced to tetramethylsilane (TMS).

X-ray photoelectron spectra (XPS): XPS Analysis was performed using a Thermo Fisher Nexsa XPS system. All XPS spectra were calibrated using the C 1s peak of carbon present at 284.80 eV.

Power X-ray diffraction (PXRD): PXRD patterns were collected on an X-ray diffraction (XRD) system (D/max-Ultima IV) using Cu Kα radiation.

Sorption isotherm for N_2: The Brunauer-Emmett-Teller (BET) surface areas were calculated from N_2 sorption isotherms at 77 K using a Micromeritics ASAP 2460 3.01 system surface area and pore size analyzer.

Thermogravimetric analysis (TGA): TGA was performed using a Netzsch TG 209 F3 Tarsus under flowing N_2 with a 20 K min^{-1} ramp rate. Samples were heated in a crucible (30-800 °C, 20 °C min^{-1}).

Scanning electron microscope (SEM): SEM images were collected using a GeminiSEM 500 system.

Transmission electron microscope (TEM): TEM images were obtained with a Tecnai G2 F30 S-Twin.

The atomic force microscopystudy (AFM): AFM images were obtained using a Bruker

Dimension Icon atomic force microscope with an Au probe.

Ultraviolet-visible (UV-vis) absorption spectra: The UV-vis absorption spectra were recorded on a Shimadzu UV-3600 plus spectrophotometer. The band gap width of the material is calculated using the Tauc plot method and extrapolating the straight-line part to the intersection of the abscissa.

Open Z-scan technology: The laser used in the experiment was an A-mode-locked Nd: YAG 532 nm laser, the ENERGY probe is Rj-7620 ENERGY RATIOMETER, the detection wavelength is 532 nm, the pulse width is 4 ns, the laser pulse energy is 5-15 μJ, and the focal spot beam waist radius is 30 μm. After passing through the attenuator, the incident light is divided by a beam splitter and focused by a lens with a focal length of 300 mm before hitting the sample. The sample moves along the optical path near the focal point of the lens, and the transmittance is monitored by two energy detectors.

DFT calculation: The structure optimizations were performed using the Gaussian 16 package, and the density functional (DFT) method B3LYP-D3(with the default D3 dispersion correction proposed by Grimme) with the 6-31G(d) basis-set. To perform the quantum mechanics calculation for the COF material, the model was constructed by extracting a unit from the COF material, and the boundaries of the truncated unit were capped with hydrogen atoms. The HOMO/LUMO and their energies were computed at the B3LYP-D3/6-31G(d) level.

2. Z-scan technique

The Z-scan technique is the most widely used method in third-order NLO research due to its simple setup, high sensitivity, wide applicability, and capability to simultaneously determine the nonlinear refractive index and nonlinear absorption coefficient of materials.

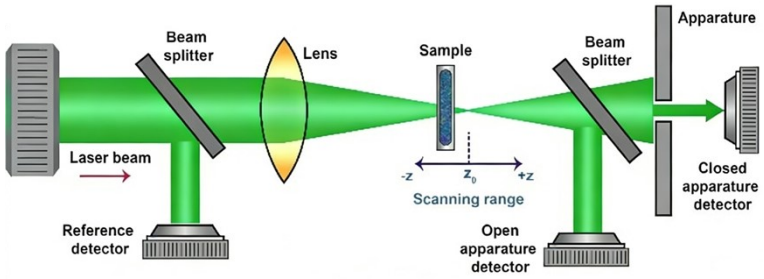

Fig. S1. Z-Scan Schematic[1].

Herein, the Z-scan technique was adopted to test the third-order NLO performance of the as-prepared samples, with the relevant calculation formulas shown as follows[2-4].

The incident laser energy:

$$E = 5E_0/T \#S - 1$$

Where E_0 is the pulse energy, and T is the linear transmittance.

The instantaneous laser intensity at the focal point:

$$I_0 = \frac{2E}{\tau\omega_0^2\pi^{3/2}} \#S - 2$$

Where τ is the pulse width of the laser pulse and ω_0 is the beam waist radius of the focal spot.

The linear absorption coefficient:

$$\alpha_0 = -\frac{ln\,(I_{out}/I_{in})}{L} \#S - 3$$

Where I_{in} is the intensity of the light incident on the sample, I_{out} is the intensity of the light emerging from the rear end of the sample, and L is the thickness of the sample, I_{out}/I_{in} is the linear transmittance of the sample according to the Beer-Lambert law.

The effective thickness of the sample:

$$L_{eff} = \frac{1 - e^{-\alpha_0 L}}{\alpha_0} \#S - 4$$

The normalized transmittance formula for the open-aperture Z-scan:

$$T(z) = 1 - \frac{\beta I_0 L_{eff}}{\left(1 + (z/z_0)^2\right)\sqrt{8}} \#S - 5$$

This formula is used to fit the open-aperture Z-scan curve, where $\beta I_0 L_{eff}$ and z/z_0 are the fitting parameters. The nonlinear absorption coefficient β is calculated using the obtained fitting parameters. β can be either positive or negative, and its sign merely indicates the third-order NLO absorption behavior of the material.

The nonlinear refractive index:

$$n_2 = \frac{\lambda\Delta T_{P-V}}{0.812\pi(1 - S)^{0.25} I_0 L_{eff}} \#S - 6$$

Where λ is the laser wavelength, $^{\Delta T_{P-V}}$ is the difference between the peak and valley of the closed-aperture Z-scan curve, and S is the linear transmittance of the aperture.

The third-order nonlinear susceptibility is a complex quantity:

$$\chi^{(3)} = \chi_R^{(3)} + i\chi_I^{(3)} \#S-7$$

Where the real part $\chi_R^{(3)}$ corresponds to the nonlinear refractive index:

$$\chi_R^{(3)} = \frac{n_0 c n_2}{80\pi} \#S-8$$

And the imaginary part $\chi_I^{(3)}$ corresponds to the two-photon absorption coefficient:

$$\chi_I^{(3)} = \frac{n_0^2 \varepsilon_0 c^2 \beta}{\omega} \#S-9$$

Here, n_0 is the refractive index of the solvent, ε_0 is the vacuum permittivity, ω is the optical frequency, and c is the speed of light.

The magnitude of the third-order nonlinear susceptibility is obtained using the formula:

$$|\chi^{(3)}| = \sqrt{|\chi_R^{(3)}|^2 + |i\chi_I^{(3)}|^2} \#S-10$$

3. Synthesis and general procedures

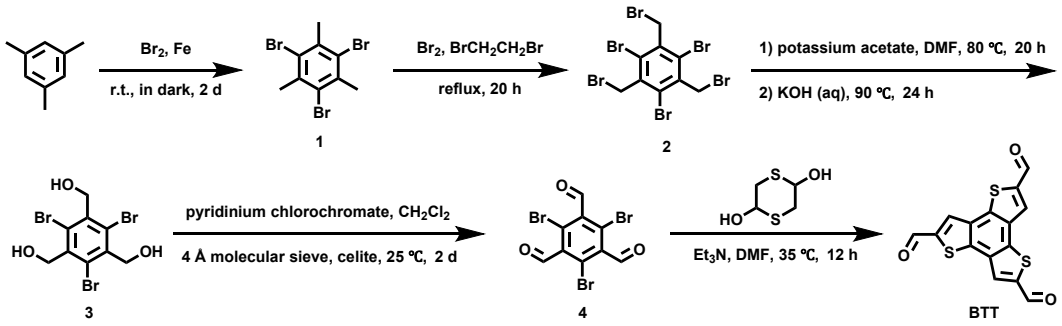

Scheme S1. Synthesis of benzo[1,2-b:3,4-b':5,6-b'']trithiophene-2,5,8-tricarbaldehyde (BTT).

1,3,5-Tribromo-2,4,6-trimethylbenzene (1).

This product was prepared based on the reported literature and was appropriately adjusted[5]. To a 250 mL three-necked round-bottom flask equipped with a gas scrubber were added iron powder (0.9 g, 16.0 mmol) and bromine (39.4 g, 247.0 mmol) at room temperature. Mesitylene (6.0 g, 50.0 mmol) was then added dropwise slowly to the mixture at room temperature. After the addition was completed, the reaction was stirred in the dark at room temperature for 48 h. Upon completion, deionized water was added to quench the reaction, and the reddish-brown crude solid was collected by filtration. Recrystallization from chloroform afforded the title compound as colorless fine needles (13.0 g, 73.5%). ^{1}H NMR (400 MHz, $CDCl_3$) δ 2.65 (s, 9H).

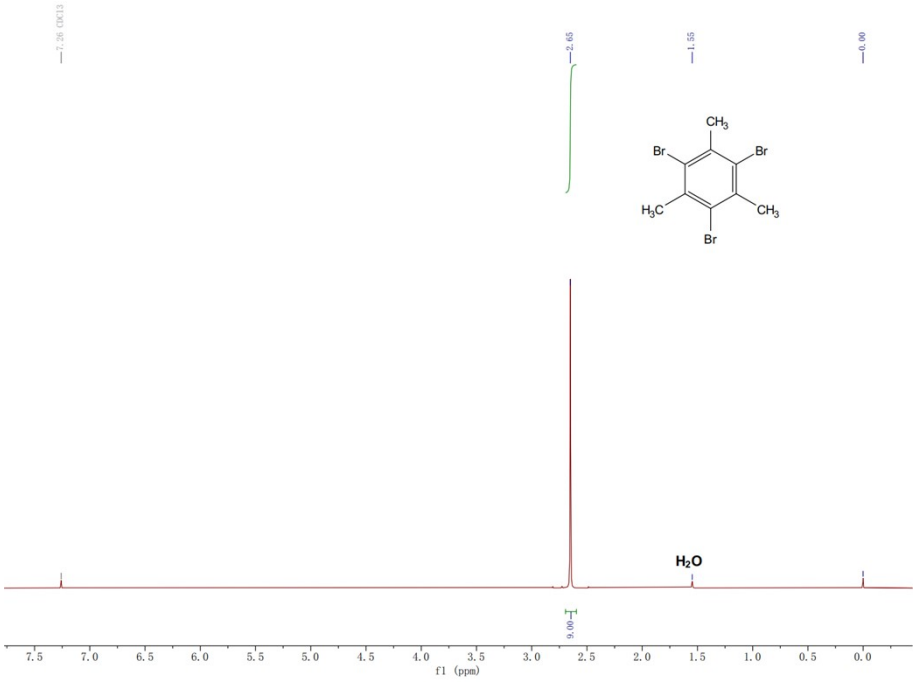

Fig. S2. ^{1}H NMR spectrum of 1,3,5-Tribromo-2,4,6-trimethylbenzene.

1,3,5-Tribromo-2,4,6-tris(bromomethyl)benzene (2).

This product was prepared based on the reported literature and was appropriately adjusted[5]. To a 250 mL three-necked round-bottom flask equipped with a gas scrubber were added 1,2-dibromoethane (25.0 mL) and **compound 1** (8.0 g, 22.0 mmol). A mixed solution of 1,2-

dibromoethane (10.0 mL) and liquid bromine (20.0 g, 126.0 mmol) was added dropwise slowly at room temperature. After the addition, the mixture was heated to reflux and stirred for 20 h. The reaction mixture was cooled to room temperature, *n*-hexane (100.0 mL) was added, and the white solid product was collected by filtration (12.7 g, 94.9%). ^{1}H NMR (400 MHz, $CDCl_3$) δ 4.92 (s, 6H).

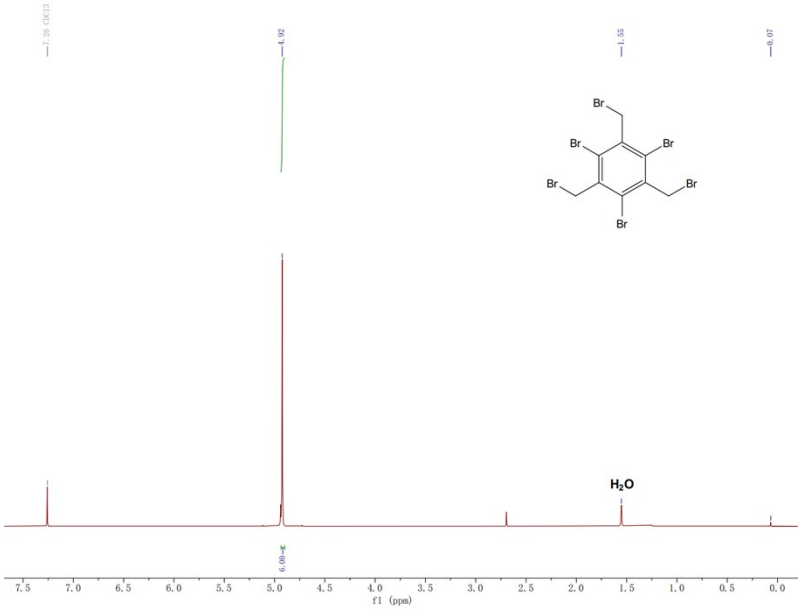

Fig. S3. ^{1}H NMR spectrum of 1,3,5-Tribromo-2,4,6-tris(bromomethyl)benzene.

1,3,5-Tribromo-2,4,6-tris(hydroxymethyl)benzene (3).

This product was prepared based on the reported literature and was appropriately adjusted[5]. To a 250 mL three-necked round-bottom flask were added **compound 2** (12.7 g, 21.5 mmol), potassium acetate (KOAc, 12.6 g, 128.5 mmol), and *N*,*N*-dimethylformamide (DMF, 100.0 mL). The mixture was heated to 80 °C and stirred for 20 h. After cooling to room temperature, the mixture was extracted with dichloromethane (DCM, 3 × 50 mL). The combined organic phases were washed with saturated brine (3 × 50 mL), dried over anhydrous Na_2SO_4, filtered, and concentrated under reduced pressure to give a white intermediate solid. The obtained intermediate, potassium hydroxide (KOH, 12.1 g, 215.0 mmol), and deionized water (200.0 mL) were transferred to a 250 mL three-necked flask, and the mixture was heated to 90 °C and stirred for 24 h. After cooling to room temperature, the pH of the mixture was adjusted to neutral with 2 M hydrochloric acid, and the white solid product was collected by filtration (8.0 g, 92.3%). ^{1}H NMR (400 MHz, DMSO-d_6) δ 5.24 (t, J = 5.2 Hz, 3H), 4.88 (d, J = 4.6 Hz, 6H).

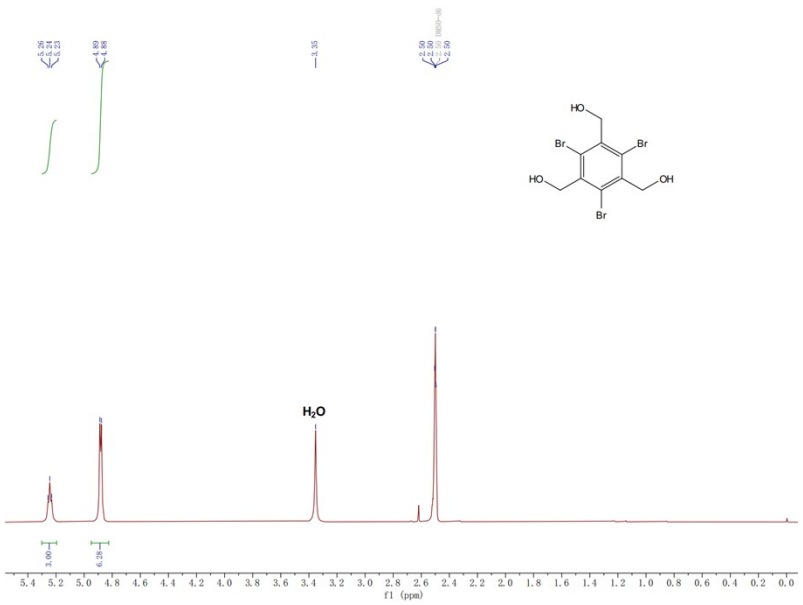

Fig. S4. ^{1}H NMR spectrum of 1,3,5-Tribromo-2,4,6-tris(hydroxymethyl)benzene.

2,4,6-Tribromo-1,3,5-benzenetricarbaldehyde (4).

This product was prepared based on the reported literature and was appropriately adjusted[5]. To a 1 L three-necked round-bottom flask were added **compound 3** (4.0 g, 10.0 mmol), pyridinium chlorochromate (PCC, 22.0 g, 102.0 mmol), 4 Å molecular sieves (12.0 g), Celite (12.0 g), DCM (500.0 mL). The mixture was stirred vigorously at room temperature for 48 h. After the reaction, the insoluble solids were removed by filtration, and the filtrate was concentrated under reduced pressure to give the crude product. Purification via silica gel column chromatography (eluent: pure DCM) afforded the title compound as a fluffy white needle-like solid (3.2 g, 81.2%).^{1}H NMR (400 MHz, DMSO-d_6) δ 10.10 (s, 3H); ^{13}C NMR (100 MHz, DMSO-d_6) δ 192.38, 137.02, 123.63.

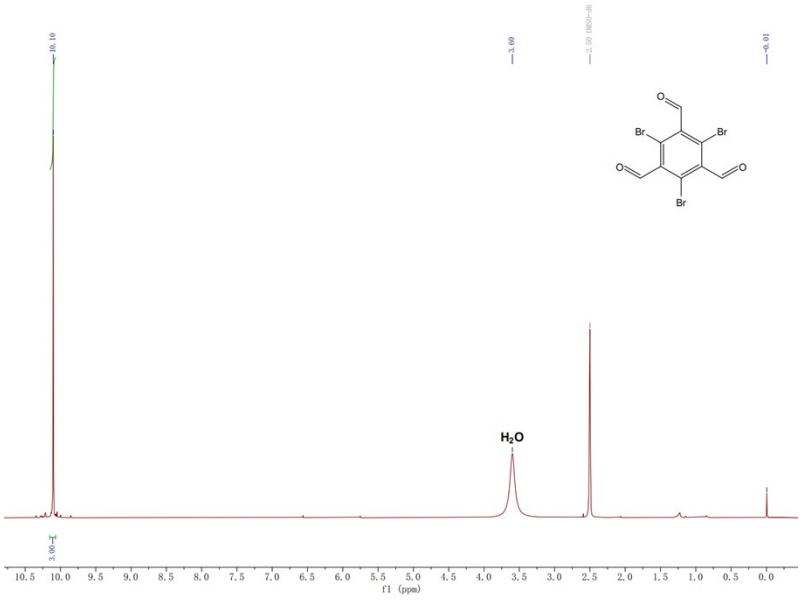

Fig. S5. ^{1}H NMR spectrum of 2,4,6-Tribromo-1,3,5-benzenetricarbaldehyde.

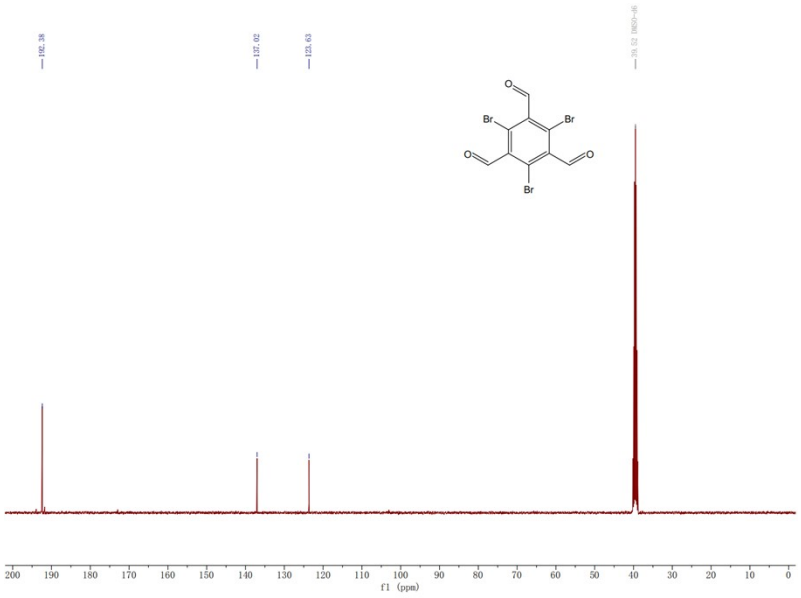

Fig. S6. ^{13}C NMR spectrum of 2,4,6-Tribromo-1,3,5-benzenetricarbaldehyde.

Benzo[1,2-b:3,4-b':5,6-b'']trithiophene-2,5,8-tricarbaldehyde (BTT).

BTT was prepared based on the reported literature and was appropriately adjusted[6]. To a 10 mL single-necked round-bottom flask were added **compound 4** (200.0 mg, 0.5 mmol), 1,4-dithiane-2,5-diol (115.0 mg, 0.8 mmol), and DMF (2.6 mL). Triethylamine (0.4 mL, 4.8 mmol) was added dropwise under an ice bath. After the addition, the mixture was heated to 35 °C and stirred for 12 h. Upon completion, the reaction mixture was poured into 50 mL of ice water, and the solid was collected by centrifugation, washed with deionized water and tetrahydrofuran several times in sequence, and dried under vacuum to afford the title compound as a light brown solid (0.1 g, 72.3%). Owing to the poor solubility of BTT in common deuterated solvents, which prevented liquid NMR characterization, model compound BMC was synthesized via Schiff-base condensation of BTT with 4-tert-butylaniline. The structural confirmation of BMC indirectly validates the successful synthesis of BTT.

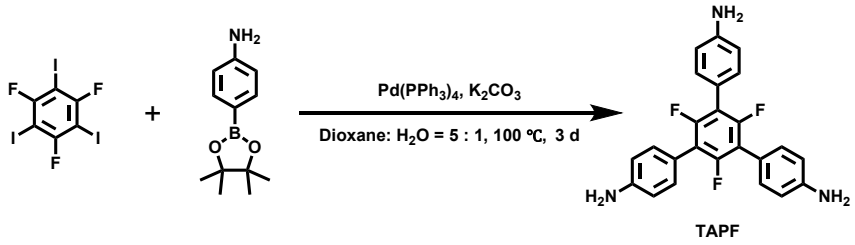

Scheme S2. Synthesis of 5'-(4-aminophenyl)-2',4',6'-trifluoro-[1,1':3',1''-terphenyl]-4,4''-diamine (TAPF).

5'-(4-aminophenyl)-2',4',6'-trifluoro-[1,1':3',1''-terphenyl]-4,4''-diamine (TAPF)

1,3,5-Trifluoro-2,4,6-triiodobenzene (0.5 g, 1.0 mmol), 4-aminophenylboronic acid pinacol ester (1.1 g, 5.0 mmol), $Pd(PPh_3)_4$ (0.1 g, 0.1 mmol), and potassium carbonate (2.0 g, 15.0 mmol) were added to a flask. Then, 1,4-dioxane: water (5:1 v/v) solution (48 mL) was added to the above mixture, followed by heating at 100 °C under nitrogen for about 3 d. After the mixture had cooled to room temperature. The residence was extracted with saturated salt water and

DCM, then the organic layer was dried with anhydrous sodium sulfate. After evaporating the solvent, the crude product was purified by column chromatography (eluent: pure DCM), and the white solid was obtained (0.32 g, 79.1%).^{1}H NMR (400 MHz, DMSO-d_6) δ (ppm) = 7.13 (d, J = 8.1 Hz, 6H), 6.64 (d, J = 8.3 Hz, 6H), 5.33 (s, 6H). ^{13}C NMR (100 MHz, DMSO-d_6) δ (ppm) = 155.86, 153.45, 148.83, 130.95, 115.08, 113.51. HRMS (ESI) m/z: Calcd for $[C_{24}H_{18}F_3N_3+H]^+$ 406.15256, found 406.1525.

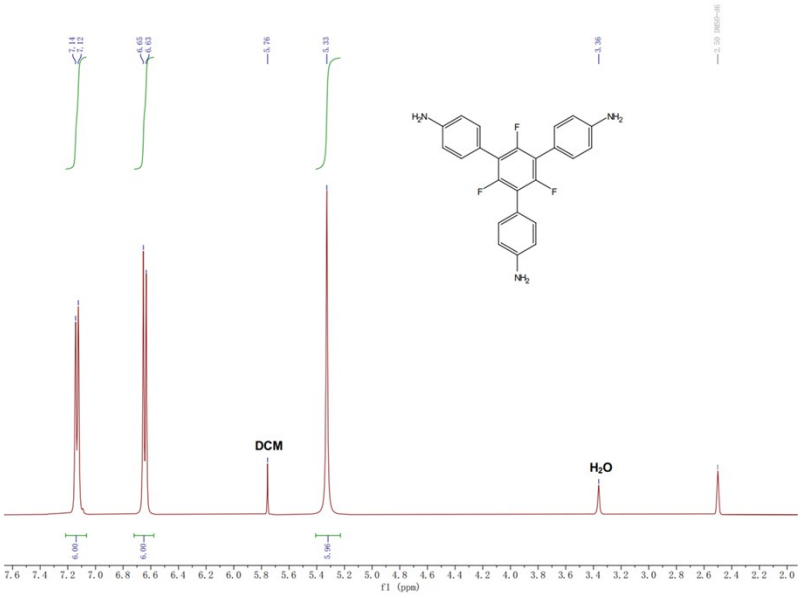

Fig. S7. ^{1}H NMR spectrum of TAPF.

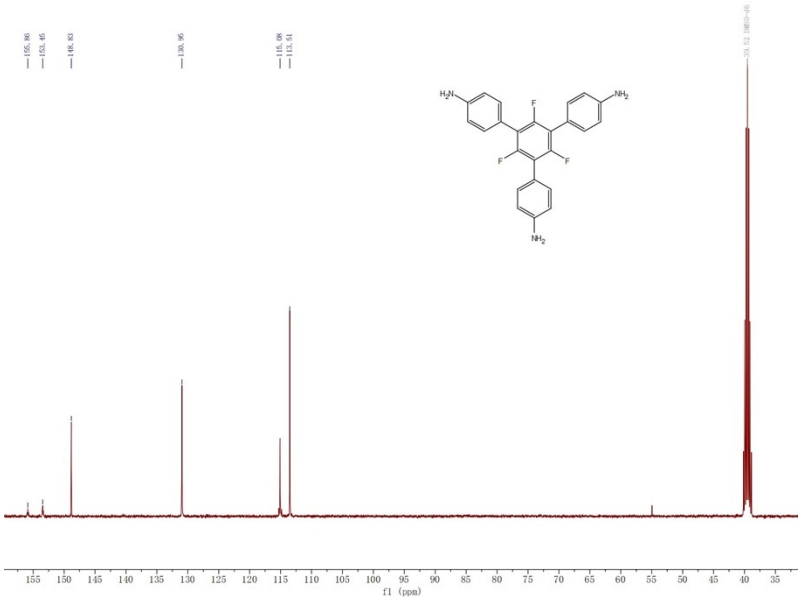

Fig. S8. ^{13}C NMR spectrum of TAPF.

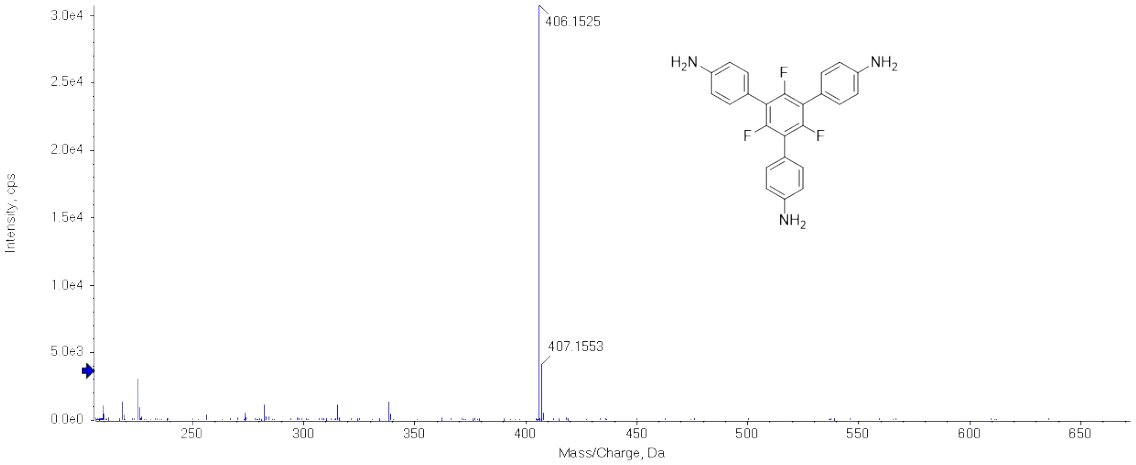

Fig. S9. HRMS spectrum of TAPF.

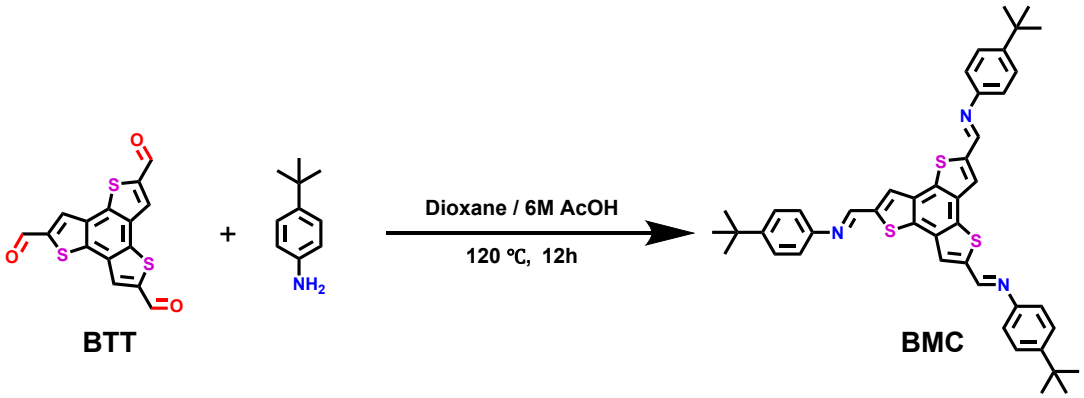

Scheme S3. Synthesis of BTT model compound (BMC)

Model compound BMC

BMC was prepared based on the reported literature and was appropriately adjusted[6]. To a 10 mL flask was added benzo[1,2-b:3,4-b':5,6-b'']trithiophene-2,5,8-tricarbaldehyde (50 mg, 0.15 mmol), 4-tert-butylaniline (86 μL, 0.54 mmol), 6M AcOH (0.05 mL), and 1,4-dioxane (1.5 mL), which was degassed three times, and the atmosphere was replaced by nitrogen. The mixture was heated at 120 °C for 12 h. After cooling to room temperature, the precipitate was filtered and recrystallized in 1,4-dioxane to obtain yellow needle like solid (66.1 mg, 61.0%). ^{1}H NMR (400 MHz, $CDCl_3$) δ (ppm) = 8.61 (s, 3H), 7.61 (s, 3H), 7.40 (d, J = 8.5 Hz, 6H), 7.23 (d, J = 8.5 Hz, 6H), 1.36 (s, 27H). ^{13}C NMR (100 MHz, $CDCl_3$) δ (ppm) = 151.76, 150.05, 148.02, 142.79, 135.27, 131.29, 126.70, 126.30, 121.15, 34.75, 31.57. HRMS (ESI) m/z: Calcd for $[C_{45}H_{45}N_3S_3+H]^+$ 724.2848, found 724.2871.

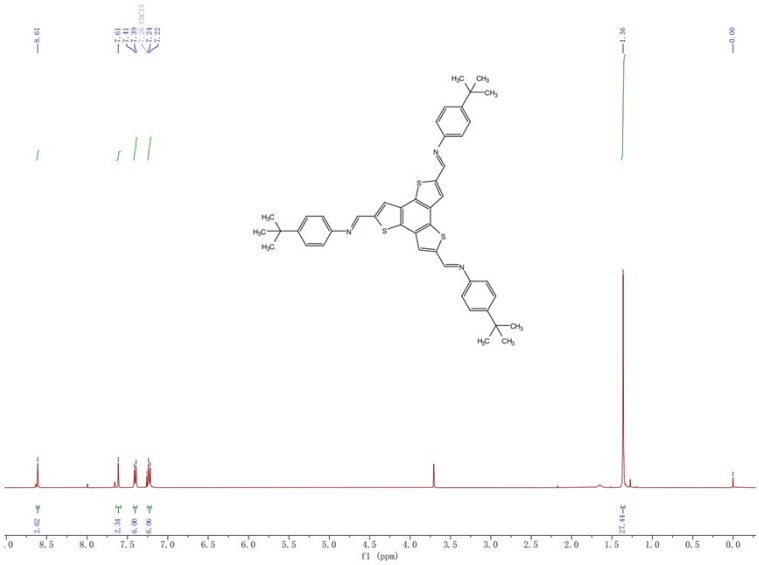

Fig. S10. ^{1}H NMR spectrum of BMC.

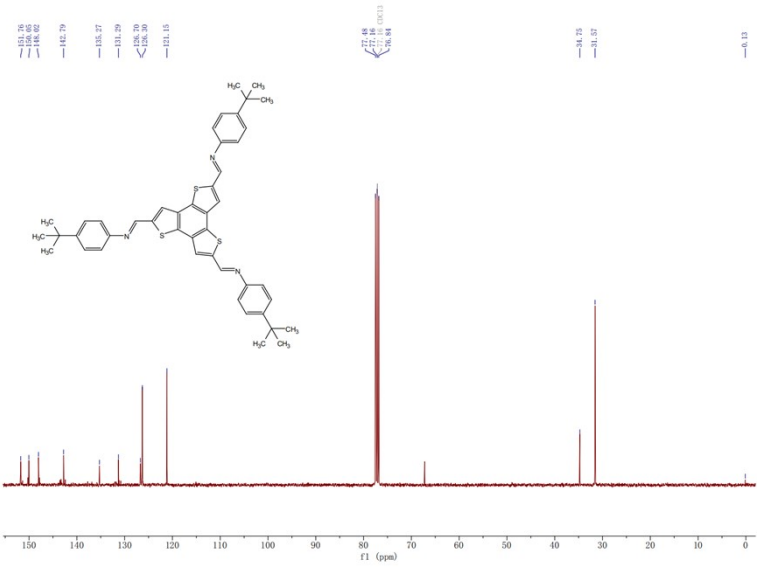

Fig. S11. ^{13}C NMR spectrum of BMC.

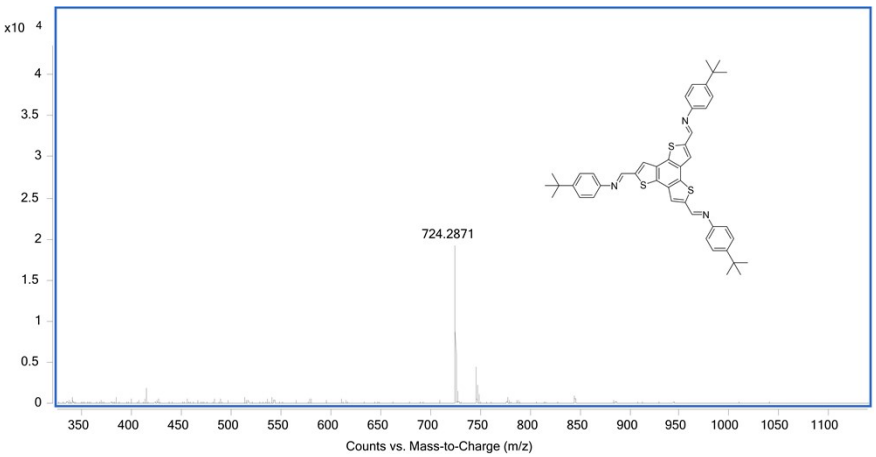

Fig. S12. HRMS spectrum of BMC

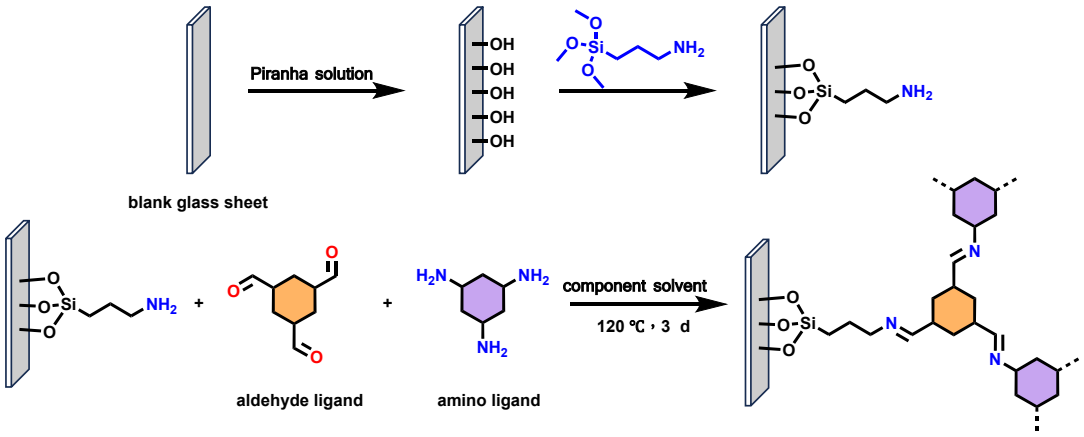

Scheme S4. Methods for synthesizing COF films.

Preparation of amino glass sheets

In this work, COF powders were synthesized via a conventional solvothermal method, and glass-supported COF films were fabricated via in situ solvothermal synthesis for the thin-film third-order NLO performance test. The in situ method employs glass as the substrate, where the interfacial confinement effect guides the oriented growth of COFs to form continuous defect-free films. However, this method has restrictions on the monomer structure, and high-rigidity monomers are hard to form uniform films on pristine glass. Thus, amination modification of glass slides was performed to improve the universality of the film-forming method[7]. Briefly, amino groups were anchored on clean glass surface, followed by Schiff-base reaction with aldehyde monomers to form an aldehyde-terminated monolayer. The COF films covalently bonded to the glass surface were then obtained via in situ Schiff-base polycondensation with amine monomers.

Aminated glass slides were fabricated following a previously reported protocol[7]. The blank glass sheets were ultrasonically cleaned with deionized water, ethanol, and ethyl acetate. After the cleaning and drying, the glass sheets were placed into a single-neck flask. Then, 20.0 mL of the piranha solution ($V_{\text{concentrated sulfuric acid}}$: $V_{\text{hydrogen peroxide}}$ = 7 : 3) was added and the mixture was immersed at 100°C for 4 hours. After 4 hours, the solution was cooled to room temperature, and the glass sheets were removed. The glass sheets were then rinsed multiple times with deionized water until neutral and dried to obtain glass sheets rich in hydroxyl groups. The hydroxylated glass sheets were placed into a single-neck flask and 27.5 mL of the 3-aminopropyltrimethoxysilane acetone solution ($V_{\text{3-aminopropyltrimethoxysilane}}$: V_{acetone} = 1 : 10) was added, followed by degassing. The mixture was replaced with nitrogen gas three times and allowed to soak for 3 days under a nitrogen atmosphere. After the reaction was complete, the sheets were rinsed with deionized water, dried, and thereby obtained amino-functionalized glass sheets.

Synthesis of BTT-COFs

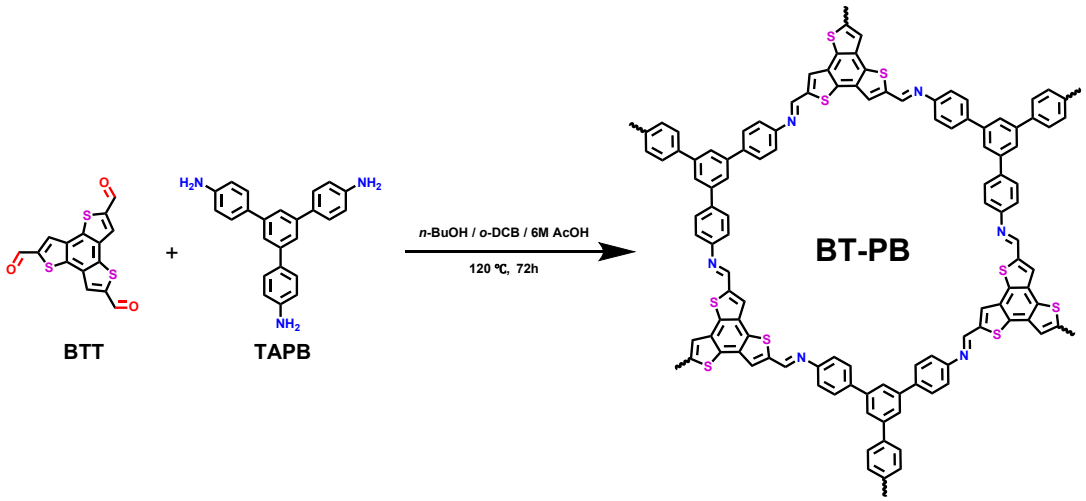

Scheme S5. Synthesis of BTT-TAPB (**BT-PB**)

BTT (40.0 mg, 0.12 mmol) and TAPB (42.6 mg, 0.12 mmol) were added to a 25 mL Schlenk tube with *o*-dichlorobenzene (2.0 mL) and *n*-butyl alcohol (2.0 mL). The mixture was sonicated for 5 minutes. Then, aminated glass sheet and 6 M acetic acid (0.4 mL) were added to the mixture. The freezing-vacuum-thaw cycle was performed three times under 77 K liquid nitrogen. The tube was sealed and heated at 120 °C for 5 days. After cooling to room temperature, the glass pane was washed with *N,N*-dimethylacetamide (DMAc) and acetone to obtain **BT-PB** film. The solid was filtered off and washed with DMF and acetone, then exhaustively washed with tetrahydrofuran and acetone by Soxhlet extraction for 48 hours. After being activated at 90 °C under a vacuum for 24 h, the yellow powder was obtained (67.8 mg, 89.1%).

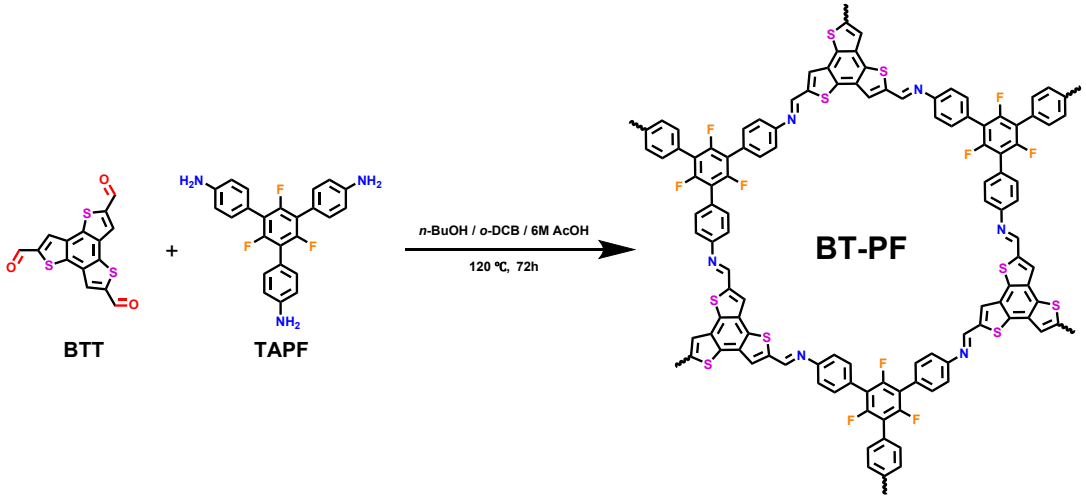

Scheme S6. Synthesis of BTT-TAPF (**BT-PF**).

BTT (36.0 mg, 0.11 mmol) and TAPF (44.2 mg, 0.11 mmol) were added to a 25 mL Schlenk tube with *o*-dichlorobenzene (2.0 mL) and *n*-butyl alcohol (2.0 mL). The mixture was sonicated for 5 minutes. Then, aminated glass sheet and 6 M acetic acid (0.4 mL) were added to the mixture. The freezing-vacuum-thaw cycle was performed three times under 77 K liquid nitrogen. The tube was sealed and heated at 120 °C for 5 days. After cooling to room temperature, the

glass pane was washed with DMAc and acetone to obtain the **BT-PF** film. The solid was filtered off and washed with DMF and acetone, then exhaustively washed with tetrahydrofuran and acetone by Soxhlet extraction for 48 hours. After being activated at 90 °C under a vacuum for 24 h, the yellow powder was obtained (65.6 mg, 83.8%).

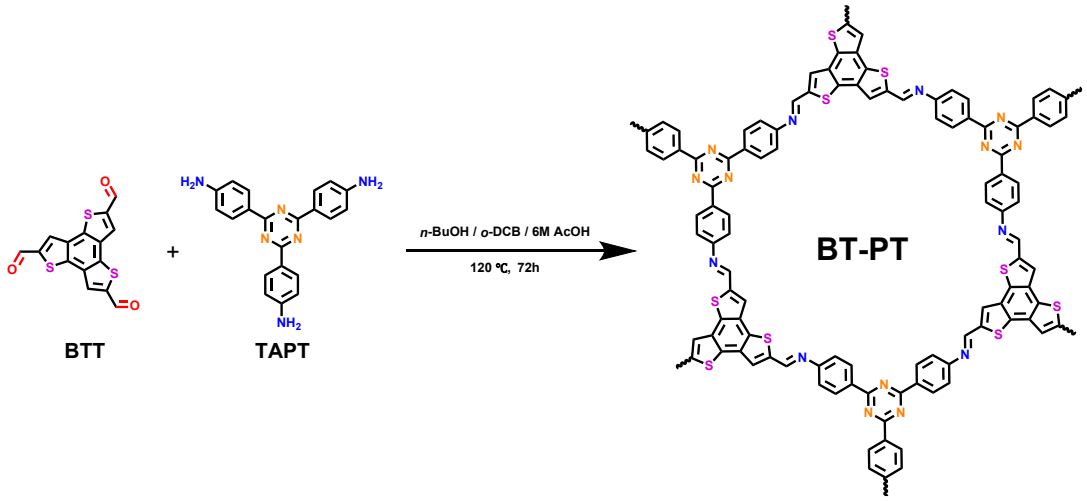

Scheme S7. Synthesis of BTT-TAPT (**BT-PT**)

BTT (40.0 mg, 0.12 mmol) and TAPT (42.9 mg, 0.12 mmol) were added to a 25 mL Schlenk tube with *o*-dichlorobenzene (2.0 mL) and *n*-butyl alcohol (2.0 mL). The mixture was sonicated for 5 minutes. Then, aminated glass sheet and 6 M acetic acid (0.4 mL) were added to the mixture. The freezing-vacuum-thaw cycle was performed three times under 77 K liquid nitrogen. The tube was sealed and heated at 120 °C for 5 days. After cooling to room temperature, the glass pane was washed with DMAc and acetone to obtain **BT-PT** film. The solid was filtered off and washed with DMF and acetone, then exhaustively washed with tetrahydrofuran and acetone by Soxhlet extraction for 48 hours. After being activated at 90 °C under a vacuum for 24 h, the yellow powder was obtained (68.8 mg, 90.0%).

4. Characterization of COFs

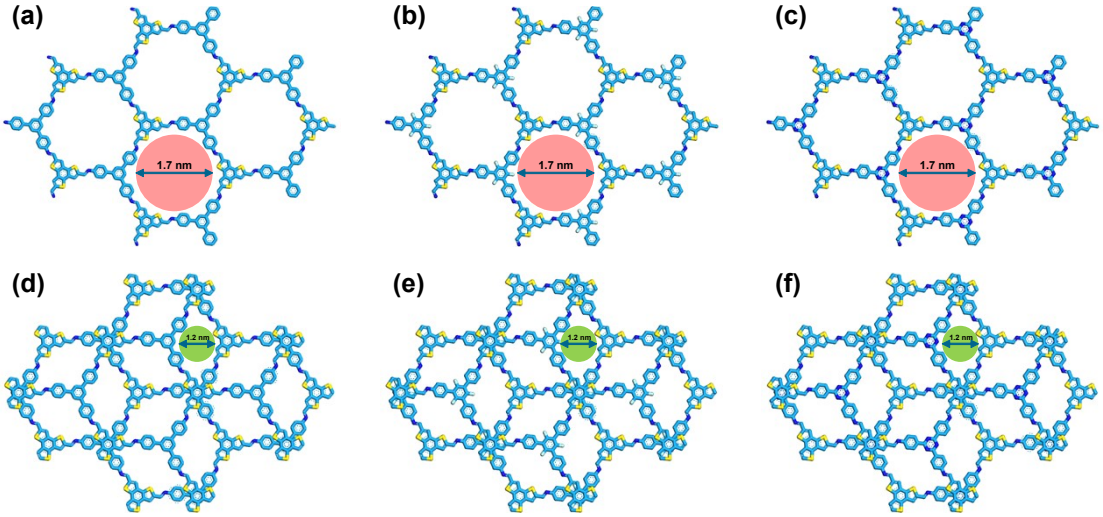

Fig. S13. AA stacking model of (a) **BT-PB**, (b) **BT-PF**, and (c) **BT-PT**; AB stacking model of (d) **BT-PB**, (e) **BT-PF**, and (f) **BT-PT**.

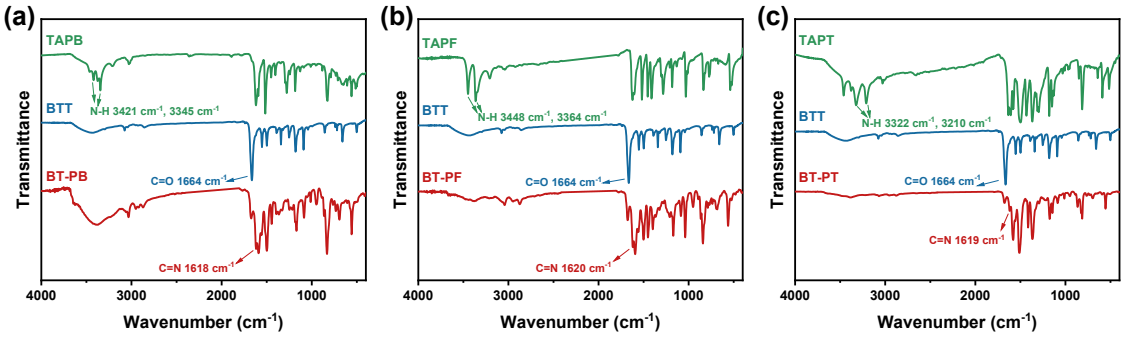

Fig. S14. FT-IR spectra of (a) **BT-PB**, (b) **BT-PF**, and (c) **BT-PT** compared with corresponding starting materials (TAPB, TAPF, TAPT, and BTT).

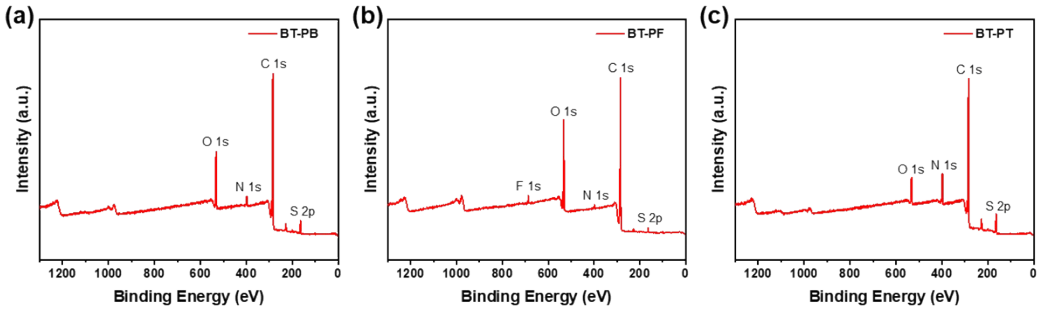

Fig. S15. XPS survey spectra of (a) **BT-PB**, (b) **BT-PF**, and (c) **BT-PT**.

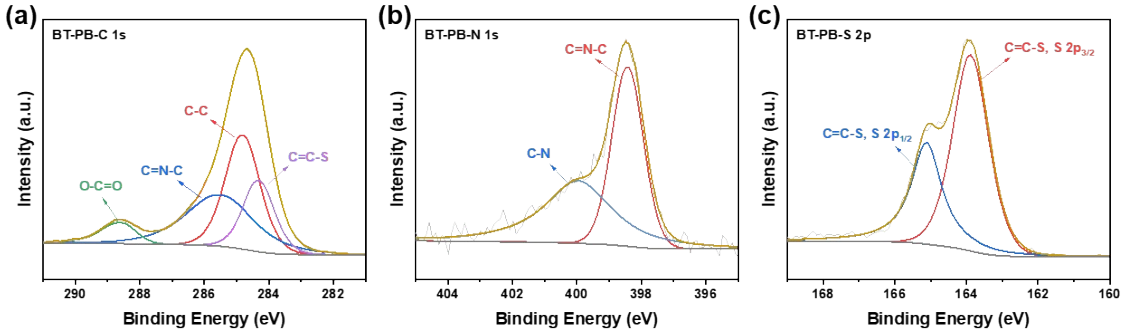

Fig. S16. XPS high-resolution spectra of **BT-PB**. (a) C 1s, (b) N 1s, and (c) S 2p.

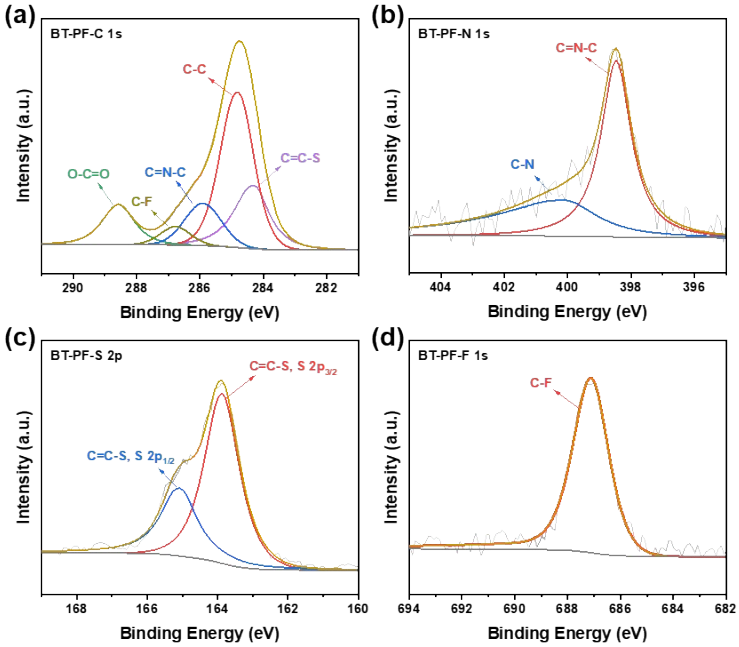

Fig. S17. XPS high-resolution spectra of **BT-PF**. (a) C 1s, (b) N 1s, (c) S 2p, and (d) F 1s.

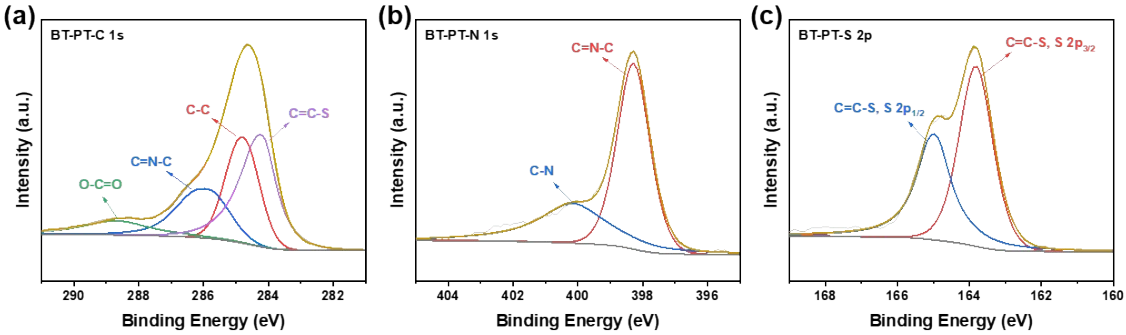

Fig. S18. XPS high-resolution spectra of **BT-PB**. (a) C 1s, (b) N 1s, and (c) S 2p.

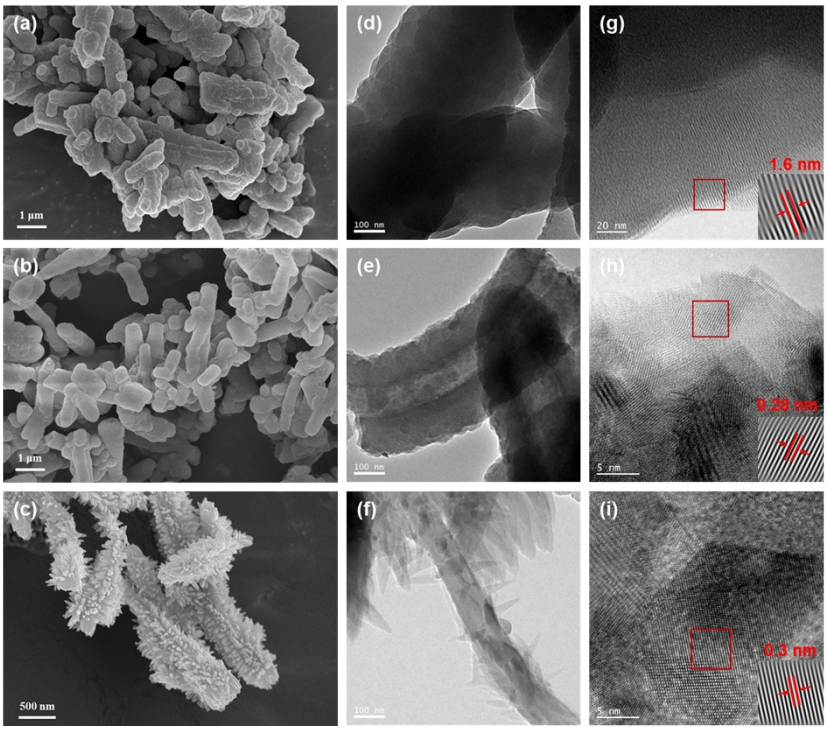

Fig. S19. SEM images of (a) **BT-PB**, (b) **BT-PF**, and (c) **BT-PT**; TEM images of (d) **BT-PB**, (e) **BT-PF**, and (f) **BT-PT**; HRTEM images of (g) **BT-PB**, (h) **BT-PF**, and (i) **BT-PT**.

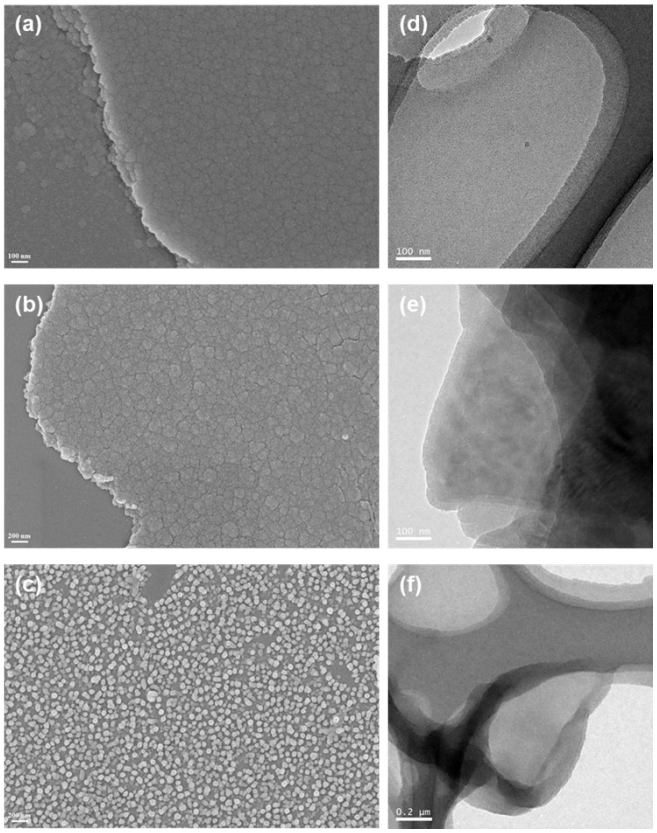

Fig. S20. SEM images of (a) **BT-PB**, (b) **BT-PF**, and (c) **BT-PT** films; TEM images of (d) **BT-PB**, (e) **BT-PF**, and (f) **BT-PT** films.

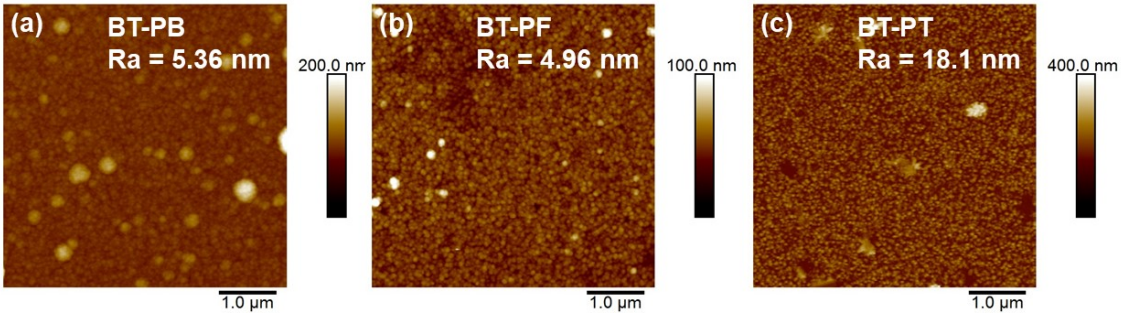

Fig. S21. AFM Roughness images of (a) **BT-PB**, (b) **BT-PF**, and (c) **BT-PT** films.

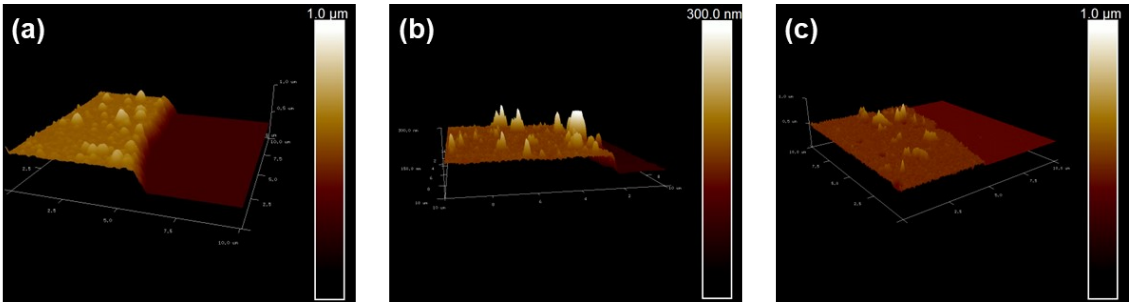

Fig. S22. AFM 3D analysis images of (a) **BT-PB**, (b) **BT-PF**, and (c) **BT-PT** films.

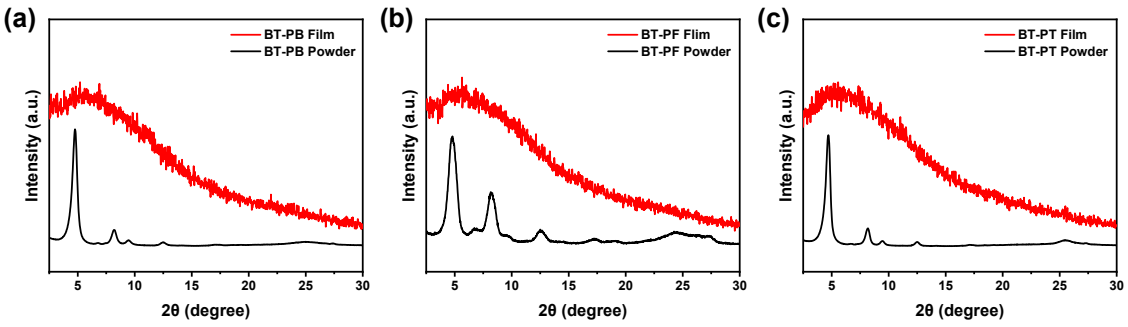

Fig. S23. XRD patterns of COFs thin films: (a) **BT-PB**, (b) **BT-PF**, and (c) **BT-PT**

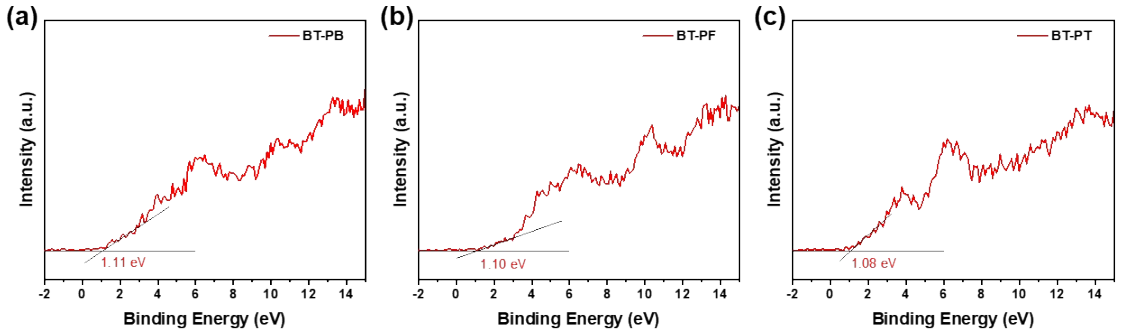

Fig. S24. Valence band (VB-XPS) spectra of (a) **BT-PB**, (b) **BT-PF**, and (c) **BT-PT**.

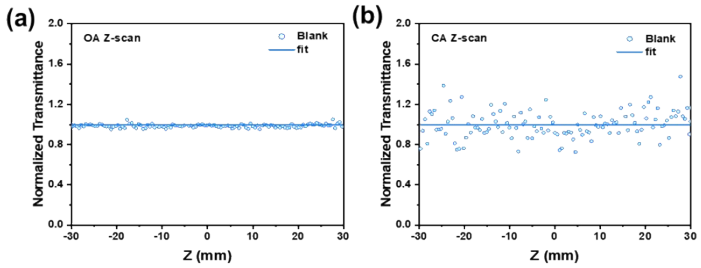

Fig. S25. (a) Open-aperture and (b) closed-aperture Z-Scan curves of pristine aminated glass substrates.

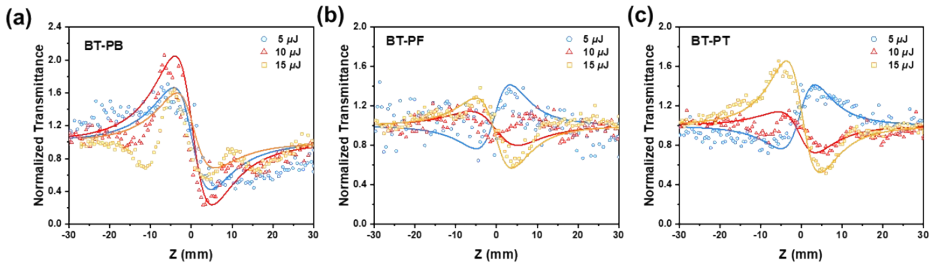

Fig. S26. Closed-aperture Z-scan curves of BT-COF films at 5, 10 and 15 μJ pulse energies.

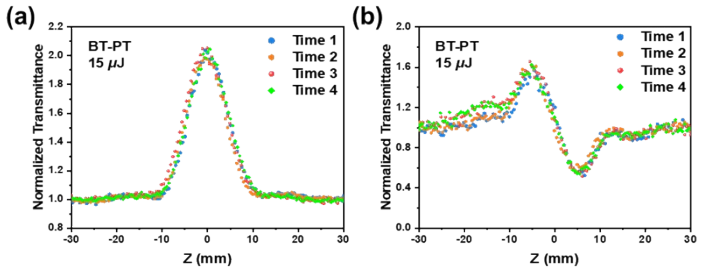

Fig. S27. Photostability measurements of BT-COF films.

Table S1. Nonlinear absorption coefficients (β) and relevant calculation parameters of BT-COFs.

Sample	Pulse energy (μJ)	Transmittance	L (nm)	L_{eff} (nm)	Fit depth	α_0 ($\times 10^{-3}$ m^{-1})	β ($\times 10^{-6}$ m/W)
BT-PB	5	0.26	297.4	163.4	−0.49	4.53	−0.31
	10				−1.88		−0.60
	15				−1.88		−0.40
BT-PF	5	0.19	83.5	40.7	−0.51	1.99	−0.95
	10				−2.28		−2.13
	15				−0.94		−0.54
BT-PT	5	0.29	88.5	50.8	−0.58	1.39	−1.33
	10				−3.00		−3.44
	15				−3.05		−2.33
	15				−3.00		−2.29
	15				−2.96		−2.26
	15				−2.96		−2.26

Table S2. Nonlinear optical properties of different materials.

Number	Materials	$\|\beta\|$	Reference
1	**BT-PB**	0.60×10^{-6} m/W	This work
	BT-PF	2.13×10^{-6} m/W	
	BT-PT	3.44×10^{-6} m/W	
2	**TFP-TZ**	1.04×10^{-6} m/W	[8]
	TF-TZ	0.12×10^{-6} m/W	
3	**Por-COF-ZnCu**	4.47×10^{-8} m/W	[9]
4	**Por-TzTz-POF**	1.10×10^{-8} m/W	[10]
5	**PMMA-PDA-InPc**	2.20×10^{-9} m/W	[11]
6	**Cu_3HHTP_2**	1.33×10^{-9} m/W	[12]
7	**PPy@Cu-MOF/PVP**	0.77×10^{-9} m/W	[13]
8	**Gu-MOF**	0.75×10^{-6} m/W	[14]
9	**DAST–PMMA**	7.44×10^{-9} m/W	[15]

Table S3. Third-order nonlinear optical performance data of BT-COFs.

COF	Pulse energy (μJ)	β (10^{-6} m W^{-1})	n_2 (10^{-13} m^2 W^{-1})	$\lvert\chi^{(3)}\rvert$ (10^{-7} esu)
BT-PB	5	−0.31	-1.83	4.95
	10	−0.60	-1.30	3.76
	15	−0.40	-0.52	1.67
BT-PF	5	−0.95	2.96	8.24
	10	−2.13	-0.76	5.27
	15	−0.54	-0.95	2.87
BT-PT	5	−1.33	3.59	10.11
	10	−3.44	-1.44	8.41
	15	−2.33	-1.98	7.51
	15	−2.29	-1.87	7.25
	15	−2.26	-1.82	7.10
	15	−2.26	-1.89	7.23

Table S4. Theoretical calculation of HOMO/LUMO energy level, energy level difference and dipole moment.

BTT-COFs	HOMO (eV)	LUMO (eV)	E_{gap} (eV)	Dipole Moment (Debye)
BT-PB	-5.52	-1.98	3.54	1.45
BT-PF	-5.56	-2.00	3.56	1.62
BT-PT	-5.68	-2.22	3.46	2.25

5. Unit cell parameters and fractional atomic coordinates

Table S5. Unit cell parameters and fractional atomic coordinates for **BT-PB** were calculated based on the AA stacking.

Space group		P6	
Calculated unit cell		*a*=*b*=22.3840 Å, *c*=3.5955 Å *α*=*β*=90°, *γ*=120°.	
Atoms	X	Y	Z
C1	1.39801	-0.32814	0.00000
C2	1.33896	-0.39250	0.00000
C3	1.35355	-0.44873	0.00000
C4	1.42107	-0.42526	0.00000
S5	1.47628	-0.33169	0.00000
C6	1.44804	-0.47283	0.00000
C7	1.59495	-0.69667	0.00000
C8	1.63607	-0.62413	0.00000
C9	1.60363	-0.57902	0.00000
C10	1.64427	-0.50662	0.00000
C11	1.61453	-0.46470	0.00000
C12	1.54294	-0.49421	0.00000
C13	1.50140	-0.56620	0.00000
C14	1.53156	-0.60773	0.00000
N15	1.51383	-0.45005	0.00000

Table S6. Unit cell parameters and fractional atomic coordinates for **BT-PF** were calculated based on the AB stacking.

Space group		P6	
Calculated unit cell		*a*=*b*=22.3696 Å, *c*=6.6434 Å *α*=*β*=90°, *γ*=120°.	
Atoms	X	Y	Z
C1	0.73242	0.34090	0.00000
C2	0.67464	0.27553	0.00000
C3	0.69154	0.22096	0.00000
C4	0.75938	0.24641	0.00000
S5	0.81248	0.34052	0.00000
C6	0.78763	0.19989	0.00000
C7	0.92838	-0.02857	0.00000
C8	0.97089	0.04394	0.00000
C9	0.94000	0.09054	0.00000
C10	0.98183	0.16294	0.00000
C11	0.95332	0.20607	0.00000
C12	0.88179	0.17778	0.00000
C13	0.83920	0.10582	0.00000
C14	0.86811	0.06317	0.00000
N15	0.85355	0.22282	0.00000
F16	1.08473	0.14105	0.00000
C17	0.39879	0.67348	0.50000
C18	0.34058	0.60837	0.50000
C19	0.35684	0.55325	0.50000
C20	0.42464	0.57807	0.50000
S21	0.47832	0.67197	0.50000
C22	0.45271	0.53135	0.50000
C23	0.59500	0.30453	0.50000
C24	0.63736	0.37704	0.50000
C25	0.60627	0.42334	0.50000
C26	0.64783	0.49576	0.50000
C27	0.61896	0.53855	0.50000
C28	0.54736	0.50983	0.50000
C29	0.50510	0.43789	0.50000
C30	0.53438	0.39563	0.50000
N31	0.51864	0.55446	0.50000
F32	0.75109	0.47454	0.50000

Table S7. Unit cell parameters and fractional atomic coordinates for **BT-PT** were calculated based on the AA stacking.

Space group		P6	
Calculated unit cell		*a*=*b*=22.1728 Å, *c*=3.5624 Å *α*=*β*=90°, *γ*=120°.	
Atoms	X	Y	Z
C1	1.39865	-0.32802	0.00000
C2	1.33908	-0.39302	0.00000
C3	1.35388	-0.44973	0.00000
C4	1.42204	-0.42599	0.00000
S5	1.47773	-0.33151	0.00000
C6	1.44927	-0.47402	0.00000
N7	1.59661	-0.69586	0.00000
C8	1.63732	-0.62558	0.00000
C9	1.60550	-0.58102	0.00000
C10	1.64748	-0.50830	0.00000
C11	1.61733	-0.46602	0.00000
C12	1.54492	-0.49581	0.00000
C13	1.50272	-0.56864	0.00000
C14	1.53289	-0.61087	0.00000
N15	1.51566	-0.45110	0.00000

References

1 S. Nath, A. Puthukkudi, J. Mohapatra and B. P. Biswal, Covalent Organic Frameworks as Emerging Nonlinear Optical Materials, *Angew Chem Int Edit*, 2023, **62**, e202218974.

2 M. Sheik-Bahae, A. Said, T. Wei, Y. Y. Wu, D. Hagan, M. Soileau and E. V. Van Stryland, Z-Scan: A Simple and sensitive technique for nonlinear refraction measurements, *Optics & Photonics*, 1990, **1148**, 41-51.

3 M. Sheik-Bahae, A. A. Said, T. H. Wei, D. J. Hagan and E. W. Van Stryland, Sensitive measurement of optical nonlinearities using a single beam, *IEEE Journal of Quantum Electronics*, 1990, **26**, 760-769.

4 J. H. Chu, T. T. Li, M. Y. Li, E. D. Su, R. Yao, H. L. Zhao, Z. Q. Li, D. B. Ding, Y. F. Yang and J. H. Jia, Regulation of nonlinear optical properties of covalent organic framework materials by imine bond orientation isomerism, *ACS Appl Energ Mater*, 2025, **9**, 160-168.

5 D. Bruns, H. Miura, K. P. C. Vollhardt and A. Stanger, En route to archimedene: Total synthesis of c3h-symmetric [7]phenylene, *Org Lett*, 2003, **5**, 549-552.

6 Z. P. Li, J. A. O. Wang, S. Ma, Z. W. Zhang, Y. F. Zhi, F. C. Zhang, H. Xia, G. Henkelman and X. M. Liu, 2D covalent organic frameworks for photosynthesis of α-trifluoromethylated ketones from aromatic alkenes, *Appl Catal B*, 2022, **310**, 121335.

7 K. Wang, H. Y. Yang, Z. Q. Liao, S. X. Li, M. Hambsch, G. Fu, S. C. B. Mannsfeld, Q. Sun and T. Zhang, Monolayer-assisted surface-initiated schiff-base-mediated aldol polycondensation for the synthesis of crystalline sp^2 carbon-conjugated covalent organic framework thin films, *J Am Chem Soc*, 2023, **145**, 5203-5210.

8 M. Y. Li, T. T. Li, C. T. Gong, D. B. Ding, J. W. Du, X. X. Zhou, Y. L. Song, Y. F. Yang, Y. B. She and J. H. Jia, Phenothiazine-based donor–acceptor covalent–organic frameworks with keto–enol irreversible tautomerism as a promising third-order nonlinear optics material, *J Mater Chem C Mater*, 2023, **11**, 13897-13904.

9 B. P. Biswal, S. Valligatla, M. Wang, T. Banerjee, N. A. Saad, B. M. K. Mariserla, N. Chandrasekhar, D. Becker, M. Addicoat, I. Senkovska, R. Berger, D. N. Rao, S. Kaskel and X. Feng, Nonlinear optical switching in regioregular porphyrin covalent organic frameworks, *Angew Chem Int Edit*, 2019, **58**, 6896-6900.

10 M. Samal, S. Valligatla, N. A. Saad, M. V. Rao, D. N. Rao, R. Sahu and B. P. Biswal, A thiazolo[5,4-*d*]thiazole-bridged porphyrin organic framework as a promising nonlinear optical material, *Chem Commun*, 2019, **55**, 11025-11028.

11 H. Zhang, L. C. Li, J. Chen, J. Wang, Y. Liu, H. J. Zhang, Q. Wang, S. Q. Wang and G. Q. Yang, Phthalocyanine covalent frameworks doped in PMMA matrix as high performance nonlinear optical limiter, *Dyes Pigm*, 2023, **219**, 111553.

12 Y. H. Sun, H. Li, X. Y. Gao, Z. Y. Yu, Z. P. Huang and C. Zhang, Superb nonlinear absorption of triphenylene-based metal–organic frameworks associated with abundant metal d electrons, *Adv Opt Mater*, 2021, **9**, 2100622.

13 Y. P. Sun, W. J. Xu, F. F. Lang, H. R. Wang, F. F. Pan and H. W. Hou, Transformation of SBUs and synergy of mof host–guest in single crystalline state: ingenious strategies for modulating third-order NLO signals, *Small*, 2023, **20**, 2305879.

14 V. Siva, A. Shameem, A. Murugan, S. Athimoolam, G. Vinitha and S. A. Bahadur, Structural, thermal and electro-optical properties of guanidine based Metal-Organic Framework (MOF), *Chin*

J Phys, 2020, **68**, 764-777.

15 M. G. Zhang, X. D. Xu, J. R. Liu, Y. D. Jiang, J. Wang, N. N. Dong, C. D. Chen, B. H. Zhu, Y. N. Liang, T. Fan and J. Xu, All-organic composite films for high flexibility and giant nonlinear optical limiting responses, *ACS Appl Mater Interfaces*, 2022, **14**, 33787-33796.